Carbohydrate Polymers 101 (2014) 75–82

Contents lists available at ScienceDirect

Carbohydrate Polymers

journal homepage: www.elsevier.com/locate/carbpol

Use of carboxylated cellulose nanofibrils-filled magnetic chitosan hydrogel beads as adsorbents for Pb(II)

Yiming Zhou [a], Shiyu Fu [a,*], Liangliang Zhang [a], Huaiyu Zhan [a], Mikhail V. Levit [b]

[a] State Key Laboratory of Pulp and Paper Engineering, South China University of Technology, Guangzhou, Guangdong 510640, China
[b] School of Chemistry and Biochemistry, Georgia Institute of Technology, Atlanta, GA 30032, United States

ARTICLE INFO

Article history:
Received 7 March 2013
Received in revised form 21 June 2013
Accepted 21 August 2013
Available online 10 September 2013

Keywords:
Magnetic chitosan hydrogel
Carboxylated cellulose nanofibrils
Heavy metals
Adsorption

ABSTRACT

Novel magnetic hydrogel beads (m-CS/PVA/CCNFs), consisting of carboxylated cellulose nanofibrils (CCNFs), amine-functionalized magnetite nanoparticles and poly(vinyl alcohol) (PVA) blended chitosan (CS), were prepared by an instantaneous gelation method. SEM, XRD, and TGA techniques were applied to investigate the structure of the hydrogel materials. The magnetic hydrogels were employed as absorbents for removal of Pb(II) ions from aqueous solutions and the fundamental adsorption behavior was studied. Experimental results revealed that the m-CS/PVA/CCNFs hydrogels exhibit higher adsorption capacity with the value of 171.0 mg/g, and the carboxylate groups on the CCNFs surface play an important role in Pb(II) adsorption. Moreover, adsorption isotherm data were reliably described by the Langmuir model and the adsorption kinetics closely followed pseudo-second order model. Additionally, the Pb(II)-loaded m-CS/PVA/CCNFs hydrogels could be easily regenerated in weak acid solution and the adsorption effectiveness of 90% can be maintained after the 4 cycles.

1. Introduction

Water contamination by heavy metals has become a major global environmental problem with the rapid development of the modern industry. Heavy metals are highly toxic at low concentrations and can accumulate in living organisms, causing various disorders and diseases (Liu, Hu, Fang, Zhang, & Zhang, 2009; Xu et al., 2011; Zhu, Fu, et al., 2012; Zhu, Hu, et al., 2012). Therefore, it is imperative to reduce or eliminate the amount of heavy metals in industrial effluent discharged into the environment. In recent years, growing attention was paid to polymer adsorbents because of their high efficiency at low concentration sewage, relatively simple process and reusability. Among the adsorbents used for the removal a number of heavy metals, many researchers give priority to low-cost natural polysaccharide materials, such as chitosan, cellulose, and starch (Pan & Ragauskas, 2012; Xie, Shang, Liu, Hu, & Liao, 2011; Zhou, Wang, Liu, & Huang, 2009). Chitosan (CS), a linear polysaccharide consisting of $\beta(1 \rightarrow 4)$ linked D-glucosamine residues with a variable number of randomly located N-acetyl-glucosamine groups is one of the high performance biomass materials. It is derived by deacetylation of chitin, the second most abundant natural polymer in the world (Muzzarelli & Muzzarelli, 2005; Varma, Deshpande, & Kennedy, 2004). Several other efficient chitosan-based adsorbents have already been explored primarily due to the fact that chitosan exhibits excellent chelating effects containing abundant hydroxyl and amino groups on the chain backbone (Merrifield, Davids, MacRae, & Amirbahman, 2004; Qu et al., 2009; Wan Ngah, Teong, & Hanafiah, 2011). However, pure chitosan materials have some significant drawbacks, such as poor chemical stability, low mechanical strength and complicated recovery process. In addition, crosslinked chitosan adsorbents were shown to have lower adsorption capacity when compared to free chitosan, because of the functional amino groups being utilized in cross-linking (Osifo et al., 2008; Wang & Wang, 2008).

Combining two or more polymers has become an increasingly interesting technique for the development of new biomaterials, which often exhibit combinations of properties that could not be achieved by an individual polymers. Chitosan blended with cellulose nanowhiskers (CNWs) or nanofibrils (CNFs) has been reported to have enhanced mechanical and chemical properties because of the strong reinforcement effect of the nanosized cellulose (Cha, He, & Ni, 2012; Spagnol et al., 2012). However, these nanocellulose materials are often obtained by strong acid hydrolysis, which removes the most amorphous regions of native cellulose and produces CNWs or CNFs with small aspect ratio. Besides, in H_2SO_4 hydrolysis, sulfate groups are

Abbreviations: CS, chitosan; CCNFs, carboxylated cellulose nanofibrils; m-CS/PVA/CCNFs, magnetic-chitosan/poly(vinyl alcohol)/CCNFs hydrogel beads; m-CS/PVA, magnetic-chitosan/poly(vinyl alcohol) hydrogel beads; CS/PVA, chitosan/poly(vinyl alcohol) hydrogel beads; SEM, scanning electron microscopy; XRD, X-ray diffraction; TGA, thermogravimetric analysis; TEMPO, 2,2,6,6-tetramethylpiperidine-1-oxyl radical; CNWs, cellulose nanowiskers; CNFs, cellulose nanofibrils; MCC, microcrystalline cellulose.

* Corresponding author. Tel.: +86 20 87112453; fax: +86 20 22236078.
E-mail addresses: shyfu@scut.edu.cn, shiyufu@gic.ac.cn (S. Fu).

0144-8617/$ – see front matter © 2013 Elsevier Ltd. All rights reserved.
http://dx.doi.org/10.1016/j.carbpol.2013.08.055

introduced to the cellulose fiber, which has negative implications for further applications (Hubbe, Rojas, Lucia, & Sain, 2008). It was recently reported that carboxylated cellulose nanofibrils (CCNFs) may find application in nanocomposite field. CCNFs can be obtained using an environmentally friendly way of combining of 2,2,6,6-tetramethylpiperidine-1-oxyl radical (TEMPO)-mediated oxidation (conditions: pH 10 and room temperature) and mechanical homogenizing. Significant amounts of carboxylate groups are formed on the CCNFs surface because of the regioselective oxidation of primary hydroxyl groups to carboxylate groups (Isogai, Yanagisawa, & Isogai, 2009; Saito, Kimura, Nishiyama, & Isogai, 2007). Furthermore, the characteristics of high mechanical strength and stiffness, excellent dispersion stability, and the ability to form a percolated network among the nanosized moieties also made CCNFs a potential reinforcing nanofiller in polymeric matrices (Fukuzumi, Saito, Iwata, Kumamoto, & Isogai, 2009; Li, Renneckar, & Barone, 2010). Despite these advantages, the use of CCNFs as nanofillers in chitosan matrices is poorly explored. Therefore, the aim of this work is to prepare nanocomposite hydrogels made of CCNFs and chitosan, and evaluate their application for heavy metal ions removal from wastewater streams. Additionally, chitosan blended with PVA can easily create a three-dimensional network without any chemical cross-linking, which is beneficial for subsequent heavy metal adsorption (Liang, Liu, Huang, & Yam, 2009).

The application of magnetic adsorbents technology has became one of the promising ways to solve environmental problems (Feng et al., 2010; Liu et al., 2009; Ozay, Ekici, Baran, Aktas, & Sahiner, 2009). Efficient separation of the adsorbents from wastewater, prior to recycling of both the sorbates and adsorbents, is a crucial step especially when the adsorbent produces particles of very small size. In the present study, CCNFs-filled magnetic chitosan hydrogel beads (m-CS/PVA/CCNFs) were prepared by an instantaneous gelation method and characterized by SEM, XRD and TGA methods. The fundamental adsorption behaviors for Pb(II) ions onto magnetic hydrogels from aqueous solution were investigated in detail. The effects of parameters such as pH, adsorbent dosage, and contract time, on the adsorption properties were studied. Moreover, the equilibrium isotherms and adsorption kinetics models were evaluated to analyze the adsorption process. The reusability study of the adsorbents was also performed.

2. Experimental

2.1. Materials

Chitosan with 91.5% degree of deacetylation and viscosity average molecular weight of 2.0×10^5 was purchased from Shandong Aokang Biological Co., Ltd. (Shandong, China). Analytical grade poly(vinyl alcohol) (98% hydrolyzed) was supplied by Shanghai Chemical Reagent Co., Ltd. (Shanghai, China). $Pb(NO_3)_2$ was obtained from Tianjin Chemical Co., Ltd. (Tianjin, China) and was used as source for Pb^{2+} ions. A stock solution of Pb^{2+} (1.0 g/L) was initially prepared, which was then diluted to desired concentrations. Other chemicals were all analytical grade and used without further purification. The deionized water was used throughout the experiments and the measured pH value was around 6.9.

2.2. Amine-functionalized magnetite nanoparticles

Amine-functionalized magnetite nanoparticles were prepared by a versatile solvothermal reaction (Wang, Bao, Wang, Zhang, & Li, 2006). $FeCl_3 \cdot 6H_2O$ (3.0 g), 1,6-hexanediamine (18.0 g), and anhydrous sodium acetate (6.0 g) were added to 120 mL of ethylene glycol, and the mixture was stirred vigorously until it turned into a transparent solution. Then this mixture was transferred to an autoclave (500 mL) and heated at 200 °C for 6 h. After the reaction, nanoparticles were recovered with the help of an adscititious magnet, and washed several times with water and ethanol, and finally dried in an oven at 70 °C.

2.3. Carboxylated cellulose nanofibrils (CCNFs)

CCNFs were prepared by two steps with a slight modification (Saito et al., 2007). Initially, 1.0 g microcrystalline cellulose (MCC, particles could pass through 200 mesh sieve) was suspended in 100 mL distilled water containing TEMPO (0.1 mmol) and NaBr (1 mmol). The oxidation process was started by adding 6% NaClO solution (5.0 mmol) under gentle agitation at room temperature. The pH of the mixture was maintained around 10.5 by adding 0.5 M NaOH and measurements using a pH-meter until no NaOH consumption was observed. Roughly, it took about 2 h to finish the oxidation reaction (Isogai et al., 2009). After that, oxidized cellulose was transferred to an ultrasonic homogenizer (JY92-IID, China) and ultrasonicated for 10 min in an ice bath with an output power of 500 W. The obtained slurry was centrifuged several times (5000 rpm, 15 min) and dialyzed against distilled water until it reached the pH of 7. The resultant product was lyophilized (−45 °C, 48 h) and stored before further use. The carboxylate content of the obtained CCNFs was determined to be 0.94 mmol/g using an electric conductivity titration method (Saito & Isogai, 2004).

2.4. Preparation of magnetic chitosan hydrogel beads

The m-CS/PVA/CCNFs hydrogel beads with a weight ratio of *W*(Chitosan):*W*(PVA) *W*(Magnetite):*W*(CCNFs) = 4:2:1:1 were prepared by an instantaneous gelation method. First, chitosan power (4.0 g) was dissolved in 100 mL 2% (v/v) aqueous acetic acid to form transparent solution at room temperature, and PVA solution was prepared by dissolving PVA power (2.0 g) in 50 mL distilled water under mechanical stirring at 70 °C. Then, PVA solution was mixed homogenously with chitosan solution, magnetite (1.0 g) and CCNFs (1.0 g) to form composite gel-forming solution with vigorous stirring for 3 h at 40 °C. After reaction, the mixture was dropped through a syringe needle into a NaOH bath (1000 mL, 0.1 M), and spherical hydrogel beads were formed instantaneously. It is worth noting that the hydrogel beads can be recovered with the help of an external magnet in order to remove unreacted chemicals. After washing with distilled water for several times, the hydrogel beads were preserved in distilled water for future use. The out diameter of the resultant beads was in the range of 2–3 mm. A proposed mechanistic pathway for the synthesis of the m-CS/PVA/CCNFs hydrogels is presented in Fig. 1. The control sample (m-CS/PVA), without adding CCNFs, was prepared according to the same procedures described above.

2.5. Characterization of magnetic chitosan hydrogel beads

The size of magnetite nanoparticles and CCNFs were measured by a high-resolution scanning electron microscopy (Nova NanoSEM 430, FEI) using an accelerating voltage of 30 kV. The cross-section morphology of magnetic hydrogel beads were performed on Quanta 200 SEM system using an accelerating voltage of 3 kV. All the SEM samples were dried via lyophilization, and coated with gold using an Emitech K 550 Coater. Wide-angle X-ray diffraction (XRD) measurements were carried out using an X-ray diffractometer (Rigaku D/max-III A, Japan). The patterns with the Cu K_α radiation ($\lambda = 0.1541$ nm) at 45 kV and 100 mA were recorded in the 2θ region from 10° to 70°. Magnetization measurements were preformed with a vibrating sample magnetometer (VSM) Model 155 at room temperature and its measurement range was

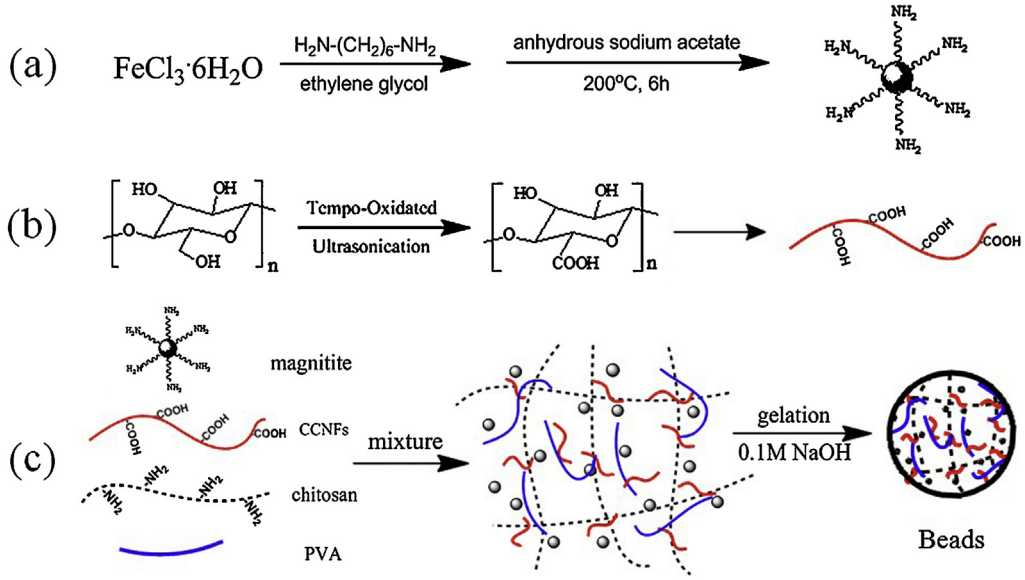

Fig. 1. Proposed mechanistic pathway for the preparation of magnetite nanoparticles (a), CCNFs (b), and m-CS/PVA/CCNFs hydrogels (c).

±10.0 kOe. Thermal stability was analyzed by a thermogravimetric analyzer (Q500, USA). 5–10 mg samples were heated from 20 to 600 °C with a heating rate of 10 °C/min under a nitrogen atmosphere of 10 cm^3/min.

2.6. Pb(II) uptake experiments

Batch adsorption experiments were conducted and equilibrated using a thermostatic shaker bath operated at 100 rpm at room temperature (25 °C). All adsorption experiments were repeated at least twice to ensure accuracy of the obtained data. The Pb(II) ions concentrations in the solutions were analyzed with an atomic absorption spectrophotometer (ZEEnit 700, German). The amount of Pb(II) adsorbed, q_e (mg/g), was calculated according to the following equation:

$$q_e = (C_0 - C_e)V/m \quad (1)$$

where C_0 and C_e (mg/L) are the initial and equilibrium Pb(II) concentrations, respectively, V (L) is the volume of the Pb(II) solution and m (g) is the amount of the dried adsorbents used.

The influence of initial solution pH on Pb(II) adsorption by magnetic adsorbents was examined. The pH of Pb(II) solutions were adjusted with 0.01 M HCl and 0.01 M NaOH solutions and controlled from 2 to 5.5. Dried magnetic samples were weighed and immerged into each of the Pb(II) solutions (100 mL, 100 mg/L) for 12 h (far above the adsorption equilibrium time).

The equilibrium isotherm was determined by placing dried magnetic adsorbents into a series of Pb(II) solutions (100 mL) with concentrations ranged from 10 to 500 mg/L. The pH of the Pb(II) solutions were 4.5, and after adsorption process for 12 h, the residual metal ions concentration were determined.

The adsorption kinetics was analyzed by placing dried magnetic adsorbents into Pb(II) solutions (200 mL, 100 mg/L) at pH 4.5. Samples were taken out with a syringe at predetermined time intervals for the analysis of residual metal ions concentration in solutions.

2.7. Desorption and reusability experiments

Desorption studies were performed in 100 mL 0.01 M HNO_3 solutions by contacting with maximum amount of Pb(II) absorbed magnetic hydrogel beads in thermostatic shaker bath for 12 h at room temperature. After removing the adsorbents from the desorption medium, the Pb(II) concentrations were determined by atomic absorption spectrophotometer. In order to test the reusability of the magnetic hydrogel beads, these adsorption-desorption cycles were repeated four times by using the same adsorbents.

3. Results and discussion

3.1. Characterization of magnetic chitosan hydrogel beads

The detailed mechanistic scheme that shows synthesis of m-CS/PVA/CCNFs hydrogels using one-step method, instantaneous gelation of the mixture containing polymers, CCNFs and magnetite nanoparticles in alkaline solutions, was described in the experimental part. SEM images of magnetite nanoparticles, CCNFs, m-CS/PVA and m-CS/PVA/CCNFs hydrogels are presented in Fig. 2. The image of the amine functionalized magnetite nanoparticles in Fig. 2a depicts nearly monodisperse nanoparticles with approximate diameter of 80 nm, while the CCNFs (Fig. 2b) resemble tiny nanofibers (nanofibrils) which are intertwined together, with the diameters in the range from 20 to 40 nm and the lengths varying from a few micrometers to 200 nm. Most aspect ratios of CCNFs were greater than 50 based on the measurements of dimensions of a representative number of samples, nanofibrils with such aspect ratio are known to be suitable for polymer reinforcement, in order to allow for sufficient stress transfer (Cheng, Wang, Rials, & Lee, 2007). The cross-section morphologies of the m-CS/PVA (Fig. 2c) and m-CS/PVA/CCNFs (Fig. 2d) hydrogels both have a relatively homogeneous porous structure, which is indicative of magnetite nanoparticles being well dispersed in space throughout the 3D structure. The average diameters of CCNFs blended magnetic hydrogels were around 5.0–10.0 μm, which is quite smaller than that of the unblended samples (about 10.0–15.0 μm). This phenomenon may be attributed to the fact that CCNFs narrowed the voids network in hydrogels and rendered the structures denser. However, some miniature continuous holes were observed in the porous walls of CCNFs-blended magnetic hydrogels, with diameters roughly 1.0–2.0 μm. The mechanism of formation of these miniature voids may be constituted by the varying instantaneous gelation rate along the direction parallel to the CCNFs, and consequently, this rate difference causes the gaps between the adjacent CCNFs. These dense holes are expected to bring a favorable capillary effect of adsorbing heavy metal ions more effectively, therefore,

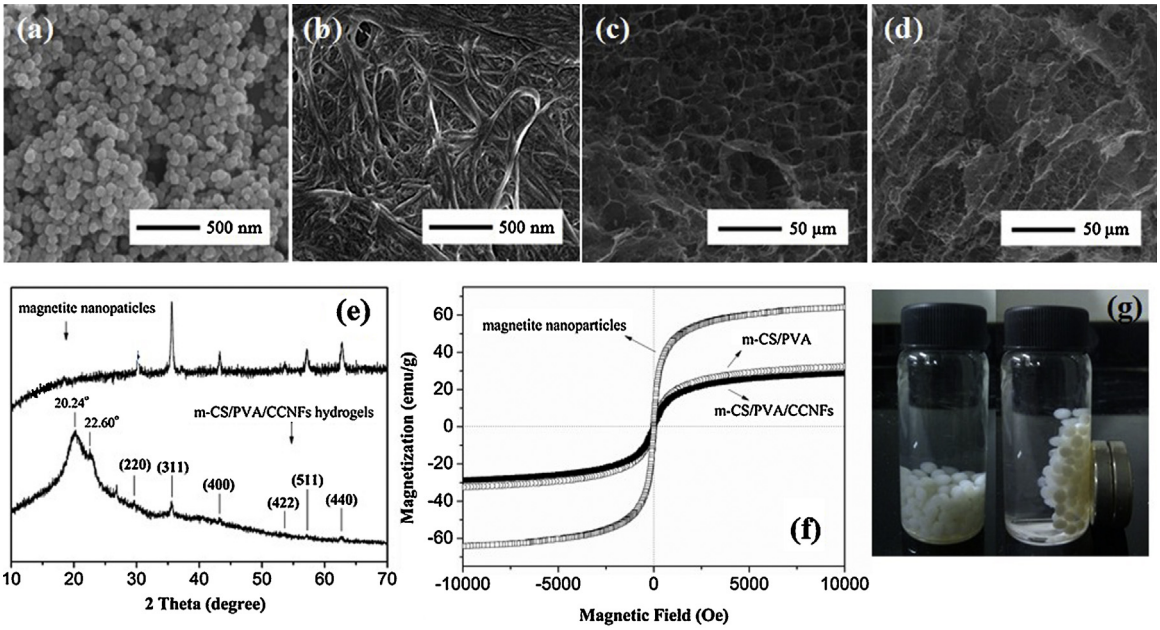

Fig. 2. SEM images of magnetite nanoparticles (a), CCNFs (b), m-CS/PVA hydrogels (c), and m-CS/PVA/CCNFs hydrogels (d), XRD patterns of magnetite nanoparticles and m-CS/PVA/CCNFs hydrogels (e), magnetization curves of magnetite nanoparticles and hydrogels at room temperature (f) and photographs of m-CS/PVA/CCNFs hydrogels in Pb(II) solution before and after magnetic separation by an external magnetic field (g).

such structure is beneficial for metal ion withholding by corresponding adsorbents.

The XRD results of magnetite nanoparticles and m-CS/PVA/CCNFs hydrogels are presented in Fig. 2e. The main peaks of magnetite nanoparticles were recorded at $2\theta = 30.23^\circ$, 35.59°, 43.27°, 53.64°, 57.20°, and 62.82°, these peaks matched well with pure magnetite reflections (JCPDS card no. 75-1610), and were consistent with the results obtained by Wang et al. (2006). At the same time, these characteristic diffraction peaks could also be found in the pattern of m-CS/PVA/CCNFs hydrogels. The strong peaks at 20.24° and 22.60° in the m-CS/PVA/CCNFs hydrogels diffractogram are related to the prominent crystallinity of chitosan and cellulose, respectively (Epure, Griffon, Pollet, & Avérous, 2011; Klemm, Heublein, Fink, & Bohn, 2005). These results indicate that the magnetic nature of m-CS/PVA/CCNFs hydrogels was validated as magnetite nanoparticles.

The magnetization curves of magnetite nanoparticles and magnetic chitosan hydrogels were recorded by VSM and illustrated in Fig. 2f. From Fig. 2f, the specific saturation magnetizations (σ_s) were 65.9, 34.5 and 31.0 emu/g for magnetite nanoparticles, m-CS/PVA and m-CS/PVA/CCNFs hydrogels, respectively. Obviously, the σ_s value of the two kinds of chitosan-based magnetic hydrogels were both much lower than that of pure magnetite nanoparticles, which was caused by the decrease in the content of magnetite nanoparticles in the nanocomposites. Moreover, σ_s of m-CS/PVA hydrogels was slightly higher than that of CCNFs blended one, which may be attributed to the increased mass of CCNFs around the magnetic nanoparticles in m-CS/PVA/CCNFs hydrogels. Such an excellent magnetic property means that as-prepared nanocomposites have strong magnetic responsivity and can be separated easily from the solution with the help of an external magnetic force. As shown in Fig. 2g, m-CS/PVA/CCNFs hydrogel beads can be completely attracted to the sidewall from the aqueous solution within about 1 min by applying an external magnet, eventually leaving the colorless and clear supernatant.

TGA curves of CS/PVA, m-CS/PVA and m-CS/PVA/CCNFs hydrogels are presented in Fig. 3a. Based on the information shown in Fig. 3a, there were two main weight loss steps in three TGA curves. The first one occurs at around 100 °C and corresponds to 5% loss in weight most likely due to the loss of adsorbed and bound water. The second stage of weight loss begins at around 245 °C for CS/PVA hydrogels and 260 °C for magnetic samples, which was associated with both the degradation of PVA and the deacetylation of chitosan (Zhu, Fu, et al., 2012; Zhu, Hu, et al., 2012). The addition of magnetite nanoparticles enhances the thermal stability of pure chitosan adsorbents, one explanation to that phenomenon can be that as metal particles stay inside the polymer networks, they can incorporate some polymer chains in their crystalline lattice preventing earlier degradation (Hernández & Mijangos, 2009). The TGA curves also show that addition of CCNFs slightly increases the thermal stability of chitosan adsorbent. This can be explained by the strong hydrogen bonding between the CCNFs and chitosan or PVA in gel formation.

3.2. pH effect on Pb(II) ions adsorption

The pH of solution is one of the key parameters that affect the adsorption process. The removal efficiency of Pb(II) ions by m-CS/PVA and m-CS/PVA/CCNFs hydrogels at various pH levels are shown in Fig. 3b. The pH range was between 2.0 and 5.5, due to the fact that when the pH is adjusted to a value higher than 5.5 lead precipitates are observed because of the increase in OH^- ion concentration in the adsorption medium. Another limitation comes from the inorganic magnetic matter starting to dissolve at pH below 2.0. As seen in Fig. 3b, at pH below 3.0, little adsorption of Pb(II) took place on both the adsorbents, especially for the m-CS/PVA. This poor adsorption performance can be caused by the presence of protonated active groups and the competition between H^+ and Pb(II) ions for adsorption sites on the adsorbents. When the pH was in the range from 3.0 to 4.5, the removal efficiency of Pb(II) rapidly increased from 18.8% to 47.3% and 36.4% to 82.4% for m-CS/PVA and m-CS/PVA/CCNFs hydrogels, respectively. However, with continued increase in pH the adsorption capacity of adsorbents for Pb(II) is somewhat decreased. Pb(II) ions may be formed as complex polynuclear species in aqueous medium, besides, chitosan will aggregate due to protonation of the amino groups in chitosan, all

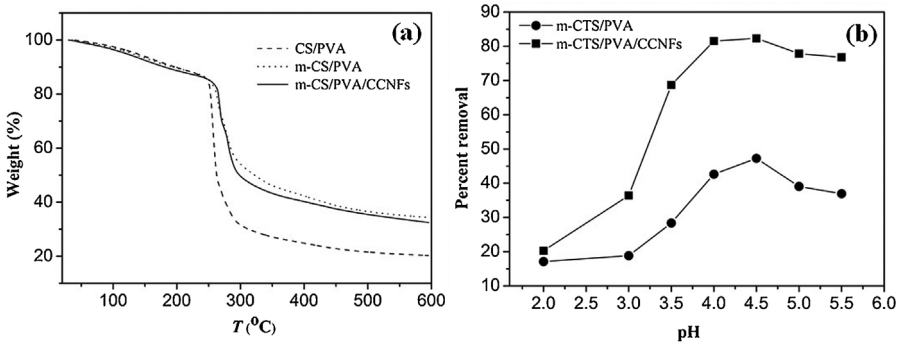

Fig. 3. TGA curves of CS/PVA, m-CS/PVA, and m-CS/PVA/CCNFs hydrogels (a), and effect of pH on the Pb(II) ions uptake by m-CS/PVA and m-CS/PVA/CCNFs hydrogels (b).

that affects chitosan affinity to Pb(II) ions, so the adsorption capacity becomes significantly lower (Liu et al., 2009). It was found that the adsorption capacity of m-CS/PVA/CCNFs hydrogels for Pb(II) was much higher than that of m-CS/PVA hydrogels throughout the entire chosen pH range, although they showed the common trend for absorption. The carboxyl groups on the CCNFs surface with concentrations of up to 0.94 mmol/g stay deprotonated as $-COO^-$ groups, which significantly enhances the electrostatic interaction between the adsorbent and metal ions.

3.3. Isotherms adsorption equilibrium

The equilibrium adsorption isotherms are fundamental in describing the interaction between the adsorbent and adsorbate. The Pb(II) adsorption isotherms for magnetic chitosan hydrogels are presented in Fig. 4a. The uptake of Pb(II) ions for both magnetic adsorbents increase linearly with the increase of ions concentration in the beginning until surface saturation is reached at higher concentration around 300 mg/L. Two common isotherm models for adsorption were used to fit experimental data.

Langmuir isotherm model is based on the assumption that adsorption sites are identical and energetically equivalent, and only monolayer adsorption occurs in the process (Langmuir, 1918). It is mathematically described as follows:

$$C_e/q_e = C_e/q_m + 1/bq_m \quad (2)$$

where q_m (mg/g) represents the maximum uptake of Pb(II) and b (L/mg) is the constant related to the energy of adsorption. q_m and b can be determined from the linear plot of C_e/q_e versus C_e.

Freundlich isotherm model is based on the assumption of exponentially decaying adsorption site energy distribution (Freundlich, 1932). It is used for heterogeneous surface energy systems and can be given as follows:

$$\ln \quad q_e = \ln \quad k_f + (\ln \quad C_e)/n \quad (3)$$

where k_f is the constant that stands for adsorption capacity related to bond strength and $1/n$ is a constant indicating adsorption intensity. k_f and n can be determined from the linear plot of $\ln q_e$ versus $\ln C_e$.

The theoretical isotherm parameters, q_m, b, k_f, n and the correlation coefficients (R^2) are listed in Table 1. The R^2 of the linear form for Langmuir model were much closer to unity than for Freundlich model. In addition, according to Langmuir model, the calculated maximum Pb(II) uptake of m-CS/PVA and m-CS/PVA/CCNFs hydrogels were quite close to their corresponding experimental data. The inset graph in Fig. 4a illustrates that experimental data fitted the theoretic Langmuir simulated curves (thin solid lines) fairly well. It revealed that Langmuir model was more reliable in describing the adsorption behavior of both magnetic chitosan for Pb(II) ions than Freundlich model, which indicated the presence of homogeneous surface in both types of adsorbents and the monolayer coverage of Pb(II) ions (Yan et al., 2012).

Furthermore, a dimensionless constant, R_L, obtained from Langmuir model is used to reflect the essential characteristic of the Langmuir model. The R_L can be calculated from the constant b (Yan et al., 2012):

$$R_L = (1 + bC_0)^{-1} \quad (4)$$

The value of R_L describes the tendency of the adsorption process, which is either unfavorable ($R_L > 1$), linear ($R_L = 1$), favorable ($0 < R_L < 1$), or irreversible ($R_L = 0$). Greater affinity between the adsorbent and the adsorbate is inferred when R_L is smaller. The R_L values were in the ranges of 0.85–0.10 for m-CS/PVA and 0.54–0.02 for m-CS/PVA/CCNFs hydrogels, which implies that the adsorption of Pb(II) ions on both magnetic chitosan hydrogels was a favorable and useful process. Moreover, the R_L value for m-CS/PVA/CCNFs hydrogels was smaller than that for m-CS/PVA ones, thus it can be concluded that the affinity of the adsorbents to Pb(II) ions is enhanced by filling them with CCNFs.

3.4. Adsorption kinetics

Fig. 4b shows the kinetics of the adsorption of Pb(II) ions by the magnetic chitosan adsorbents. Upon inspection of the uptake–time curves, it is shown that the adsorption of Pb(II) increases rapidly during the initial 50 min after the immersion, reaching about 80% of the equilibrium value, and after that, the Pb(II) uptake continues to increase slowly and remains constant after 200 min. In order to examine the mechanism ruling the adsorption process (whether the adsorption is dominated by a physical or chemical mechanism), the commonly used kinetic models: the pseudo-first order, pseudo-second order and intra-particle diffusion models were employed to examine the kinetics data. The pseudo-first order (Eq. (5)) and pseudo-second order (Eq. (6)) models are illustrated as follows (Zhou et al., 2009; Zhu, Fu, et al., 2012; Zhu, Hu, et al., 2012):

$$1/q_t = k_1/q_e t + 1/q_e \quad (5)$$

$$t/q_t = 1/k_2 q_e^2 + t/q_e \quad (6)$$

where q_t (mg/g) is the amount of Pb(II) ions adsorbed onto adsorbents at time t (min). k_1 (min^{-1}) and k_2 (g/(mg min)) are the rate constant of pseudo-first order and pseudo-second order adsorption, respectively, which can be obtained from $\log(q_e - q_t)$ versus t and t/q_t versus t, respectively.

Intra-particle diffusion equation suggests that intra-particle diffusion is the rate-limiting step in the adsorption and can be described as (Periasamy & Namasivayam, 1994):

$$q_t = k_{id} t^{0.5} + c \quad (7)$$

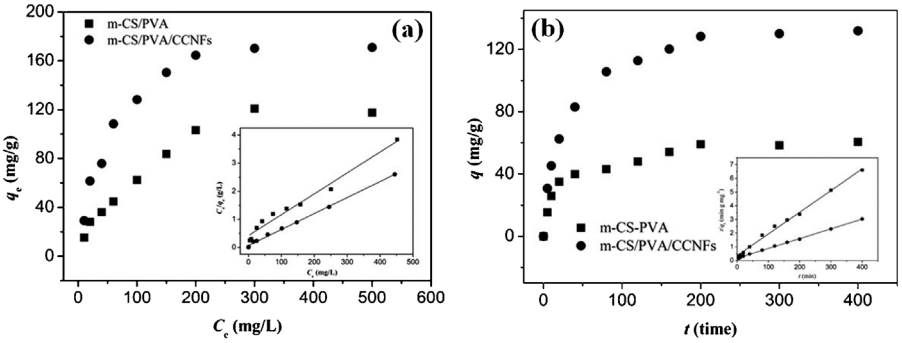

Fig. 4. Adsorption isotherms (a) and kinetics (b) of Pb(II) ions uptake on m-CS/PVA and m-CS/PVA/CCNFs hydrogels. The inset shows the fitting results by the Langmuir isothermal model (a) and pseudo-second order model (b).

Table 1
Isotherms parameters of Pb(II) ions adsorption onto magnetic chitosan adsorbents.

Adsorbents	$q_{m,exp}$ (mg/g)	Langmuir model			Freundlich model			
		$q_{m,cal}$ (mg/g)	$b \times 10^3$ (L/g)	R^2	R_L	k_f	n	R^2
m-CS/PVA	117.6	134.6	17.62	0.973	0.85–0.10	37.47	3.543	0.956
m-CS/PVA/CCNFs	171.0	175.4	84.42	0.997	0.54–0.02	9.265	2.236	0.966

Table 2
Kinetic parameters of Pb(II) ions adsorption onto magnetic chitosan adsorbents.

Adsorbents	$q_{e,exp}$ (mg/g)	Pseudo-first-order			Pseudo-second-order			Intra-particle diffusion		
		$q_{e1,cal}$ (mg/g)	k_1 (min^{-1})	R^2	$q_{e2,cal}$ (mg/g)	$k_2 \times 10^4$ (g/(mg min))	R^2	C (mg/g)	k_{id} (mg/(g min$^{0.5}$))	R^2
m-CS/PVA	60.61	43.04	0.012	0.937	63.17	6.961	0.995	20.46	2.343	0.864
m-CS/PVA/CCNFs	131.9	90.87	0.012	0.970	139.9	3.033	0.999	37.56	5.738	0.850

where c is the intercept (mg/g) and k_{id} (mg/(g min$^{0.5}$)) is the intra-particle diffusion rate constant, which can be evaluated from the slope of the linear plot of q_t versus $t^{0.5}$.

The experimental data have been fitted to the kinetics models mentioned above, and the obtained parameters are listed in Table 2. The values of the R^2 for the pseudo-second-order model were much closer to unity for both magnetic adsorbents, and the adsorption capacities calculated by the model ($q_{e2,cal}$) were also closer to those determined by experiments ($q_{e,exp}$). Moreover, the fitting results of the pseudo-second order model was shown in the inset graph of Fig. 4b. The experimental data fitted the theoretical simulated curves (thin solid lines) quite well. These results indicate that the applicability of pseudo-second-order kinetic model is feasible for describing the adsorption process of Pb(II) on the magnetic adsorbents, which suggests chemical adsorption as the rate-limiting step of the adsorption mechanism and no involvement of mass transfer in solution (Ho & McKay, 2000; Wu, Tseng, & Juang, 2001). The results were completely consistent with those drawn from adsorption isotherm analysis as previously mentioned. The R^2 values of intra-particle diffusion model obtained were much lower ($R^2 < 0.90$) compared with those obtained from pseudo-second-order kinetic model, revealing that the intra-particle diffusion was not the rate-limiting step in the adsorption.

3.5. Desorption and reusability study

The reusability of the absorbents is one of the most important features for their convincing economic feasibility and resourcefulness. Therefore, the desorption–adsorption cycles were performed to investigate the potential of m-CS/PVA and m-CS/PVA/CCNFs hydrogels for real applications. In this study, desorption studies were carried out using 0.01 M HNO_3 solution, and the final results were shown in Table 3. According to Table 3, the adsorption effectiveness of both the magnetic chitosan adsorbents could still be maintained at 90% level even after four cycles and m-CS/PVA hydrogels exhibit better reusability than CCNFs blended magnetic hydrogels. Thus, due to the high recycling potential, m-CS/PVA and m-CS/PVA/CCNFs hydrogels were both qualified for practical application.

Table 3
Desorption and reusability behaviors of Pb(II) ions onto magnetic chitosan hydrogels.

Cycle	m-CS/PVA		m-CS/PVA/CCNFs	
	Desorption (%)	Adsorption (%)	Desorption (%)	Adsorption (%)
Cycle 1	98.8	97.9	95.4	94.0
Cycle 2	97.0	96.1	94.1	92.6
Cycle 3	95.4	95.1	92.8	91.6
Cycle 4	94.8	93.2	91.4	90.1

3.6. Comparison with other chitosan adsorbents

m-CS/PVA/CCNFs hydrogels displayed magnetic properties along with improved efficiency in removal of Pb(II) ions, due to the higher affinity of the hydroxyl, amino and carboxylate groups to form stable complexes with metal ions. The q_m value of the m-CS/PVA hydrogels without adding CCNFs was 117.6 mg/g, which was lower than that of corresponding CCNFs blended magnetic hydrogels – 171.0 mg/g. These results indicate that addition of CCNFs into the magnetic chitosan hydrogels improves the adsorption behavior for the investigated Pb(II) ions. The q_m values for Pb(II) ions adsorption onto other modified chitosan adsorbents, prepared under various conditions, reported in the literature, are compared in Table 4. It can be seen that the q_m values differ considerably for several adsorbents and that, by comparison, the m-CS/PVA/CCNFs hydrogels are a promising alternative for the removal of Pb(II) from

Table 4
q_m values for Pb(II) ions adsorption for different adsorbents.

Adsorbents	q_m (mg/g)	References
m-chitosan/PVA/CCNFs	171.0	This study
m-chitosan/PVA	117.6	This study
Xanthate-modified magnetic chitosan	76.9	Zhu, Fu, et al. (2012) and Zhu, Hu, et al. (2012)
Hydrolyzed polyacrylamide-chitosan beads	353.09	Cao, Tan, Che, and Xin (2010)
Chitosan/epichlorohydrin-triphosphate	166.94	Laus, Costa, Szpoganicz, and Fávere (2010)
Chitosan/Fe_3O_4 nanocomposite beads	63.33	Tran, Tran, and Nguyen (2010)
GLA-crosslinked metal-complexed chitosans	105.26	Chen, Yang, Chen, Chen, and Chen (2009)
Chitosan-alginate beads	60.27	Wan Ngah and Fatinathan (2010)
Chitosan/TiO_2 hybrid film	36.8	Tao, Ye, Pan, Wang, and Tang (2009)

aqueous solutions mainly due to their relatively high adsorption capacity.

4. Conclusion

CCNFs-filled magnetic chitosan hydrogel beads were prepared and characterized by SEM, XRD and TGA. Analysis indicated that the magnetite nanoparticles were dispersed well in the adsorbents, thus resulting in significant improvement of the ability separated from aqueous solutions. The uptake of Pb(II) ions was further improved by blending with CCNFs due to the presence of carboxylate groups on the CCNFs surface. Adsorption equilibrium isotherms and kinetics illustrated that adsorption mechanisms in both m-CS/PVA and m-CS/PVA/CCNFs hydrogels followed a monolayer chemical adsorption process, and the affinity of the adsorbents to Pb(II) ions was enhanced after filling with CCNFs. Desorption and reuse experiments indicated that m-CS/PVA/CCNFs hydrogels could be regenerated and the adsorption level stayed at 90% even after four cycles. Overall, m-CS/PVA/CCNFs hydrogels could be considered as a promising adsorbent for the removal of Pb(II) ions for their high adsorption capacity, fine biodegradability, and ability to be rapidly separated from aqueous solutions.

Acknowledgments

The authors wish to express their gratitude for the financial support from the Ministry of Science and Technology (973 project, 2010CB732206), the Doctoral Program Foundation of Institutions of Higher Education of China (No. 20090172110022), China.

References

Cao, J., Tan, Y. B., Che, Y. J., & Xin, H. P. (2010). Novel complex gel beads composed of hydrolyzed polyacrylamide and chitosan: An effective adsorbent for the removal of heavy metal from aqueous solution. *Bioresource Technology*, *101*, 2558–2561.

Cha, R. T., He, Z. B., & Ni, Y. H. (2012). Preparation and characterization of thermal/pH-sensitive hydrogel from carboxylated nanocrystalline cellulose. *Carbohydrate Polymers*, *88*, 713–718.

Chen, A. H., Yang, C. Y., Chen, C. Y., Chen, C. Y., & Chen, C. W. (2009). The chemically crosslinked metal-complexed chitosans for comparative adsorptions of Cu(II), Zn(II), Ni(II) and Pb(II) ions in aqueous medium. *Journal of Hazardous Materials*, *163*, 1068–1075.

Cheng, Q., Wang, S., Rials, T. G., & Lee, S. H. (2007). Physical and mechanical properties of polyvinyl alcohol and polypropylene composite materials reinforced with fibril aggregates isolated from regenerated cellulose fibers. *Cellulose*, *14*, 593–602.

Epure, V., Griffon, M., Pollet, E., & Avérous, L. (2011). Structure and properties of glycerol-plasticized chitosan obtained by mechanical kneading. *Carbohydrate Polymers*, *83*, 947–952.

Feng, Y., Gong, J. L., Zeng, G. M., Niu, Q. Y., Zhang, H. Y., Niu, C. G., et al. (2010). Adsorption of Cd (II) and Zn (II) from aqueous solutions using magnetic hydroxyapatite nanoparticles as adsorbents. *Chemical Engineering Journal*, *162*, 487–494.

Freundlich, H. (1932). Of the adsorption of gases. Section II. Kinetics and energetics of gas adsorption. Introductory paper to section II. *Transactions of The Faraday Society*, *28*, 195–201.

Fukuzumi, H., Saito, T., Iwata, T., Kumamoto, Y., & Isogai, A. (2009). Transparent and high gas barrier films of cellulose nanfibers prepared by TEMPO-mediated oxidation. *Biomacromolecules*, *10*, 162–165.

Hernández, R., & Mijangos, C. (2009). In situ synthesis of magnetic iron oxide nanoparticles in thermally responsive alginate-poly(N-isopropylacrylamide) semi-interpenetrating polymer networks. *Macromolecular Rapid Communications*, *30*, 176–181.

Ho, Y. S., & McKay, G. (2000). The kinetics of sorption of divalent metal ions onto sphagnum moss peat. *Water Research*, *34*, 735–742.

Hubbe, M. A., Rojas, O. J., Lucia, L. A., & Sain, M. (2008). Cellulosic nanocomposites: A review. *Bioresources*, *3*, 929–980.

Isogai, T., Yanagisawa, M., & Isogai, A. (2009). Degrees of polymerization (DP) and DP distribution of cellouronic acids prepared from alkali-treated celluloses and ball-milled native celluloses by TEMPO-mediated oxidation. *Cellulose*, *16*, 117–127.

Klemm, D., Heublein, B., Fink, H. P., & Bohn, A. (2005). Cellulose: Fascinating biopolymer and sustainable raw material. *Angewandte Chemie International Edition*, *44*, 2–37.

Langmuir, I. (1918). The adsorption of gases on plane surfaces of glass, mica and platinum. *Journal of the American Chemical Society*, *40*, 1361–1403.

Laus, R., Costa, T. G., Szpoganicz, B., & Fávere, V. T. (2010). Adsorption and desorption of Cu(II), Cd(II) and Pb(II) ions using chitosan crosslinked with epichlorohydrin-triphosphate as the adsorbent. *Journal of Hazardous Materials*, *183*, 233–241.

Liang, S., Liu, L., Huang, Q., & Yam, K. L. (2009). Preparation of single or double-network chitosan/poly(vinyl alcohol) gel films through selectively cross-linking method. *Carbohydrate Polymers*, *77*, 718–724.

Li, Z., Renneckar, S., & Barone, J. R. (2010). Nanocomposites prepared by in situ enzymatic polymerization of phenol with TEMPO-oxidized nanocellulose. *Cellulose*, *17*, 57–68.

Liu, X. W., Hu, Q. Y., Fang, Z., Zhang, X. J., & Zhang, B. B. (2009). Magnetic chitosan nanocomposites: A useful recyclable tool for heavy metal ion removal. *Langmuir*, *25*, 3–8.

Merrifield, J. D., Davids, W. G., MacRae, J. D., & Amirbahman, A. (2004). Uptake of mercury by thiol-grafted chitosan gel beads. *Water Research*, *38*, 3132–3138.

Muzzarelli, R. A. A., & Muzzarelli, C. (2005). Chitosan chemistry: Relevance to the biomedical sciences. *Advances in Polymer Science*, *186*, 151–209.

Osifo, P. O., Webster, A., van der Merwe, H., Neomagus, H. W. J. P., van der Gun, M. A., & Grant, D. M. (2008). The influence of the degree of cross-linking on the adsorption properties of chitosan beads. *Bioresource Technology*, *99*, 7377–7382.

Ozay, O., Ekici, S., Baran, Y., Aktas, N., & Sahiner, N. (2009). Removal of toxic metal ions with magnetic hydrogels. *Water Research*, *43*, 4403–4411.

Pan, S. B., & Ragauskas, A. J. (2012). Preparation of superabsorbent cellulosic hydrogels. *Carbohydrate Polymers*, *87*, 1410–1418.

Periasamy, K., & Namasivayam, C. (1994). Process development for removal and recovery of cadmium from wastewater by a low cost adsorbent: Adsorption rates and equilibrium studies. *Industrial & Engineering Chemistry Research*, *33*, 317–320.

Qu, R. J., Sun, C. M., Wang, M. H., Ji, C. N., Xu, Q., Zhang, Y., et al. (2009). Adsorption of Au(III) from aqueous solution using cotton fiber/chitosan composite adsorbents. *Hydrometallurgy*, *100*, 65–71.

Saito, T., & Isogai, A. (2004). TEMPO-mediated oxidation of native cellulose. The effect of oxidation conditions on chemical and crystal structures of the water-insoluble fractions. *Biomacromolecules*, *5*, 1983–1989.

Saito, T., Kimura, S., Nishiyama, Y., & Isogai, A. (2007). Cellulose nanofibers prepared by TEMPO-mediated oxidation of native cellulose. *Biomacromolecules*, *8*, 2485–2491.

Spagnol, C., Rodrigues, F. H. A., Pereira, A. G. B., Fajardo, A. R., Rubira, A. F., & Muniz, E. C. (2012). Superabsorbent hydrogel composite made of cellulose nanofibrils and chitosan-graft-poly(acrylic acid). *Carbohydrate Polymers*, *87*, 2038–2045.

Tao, Y. G., Ye, L. B., Pan, J., Wang, Y. M., & Tang, B. (2009). Removal of Pb(II) from aqueous solution on chitosan/TiO_2 hybrid film. *Journal of Hazardous Materials*, *161*, 718–722.

Tran, H. V., Tran, L. D., & Nguyen, T. N. (2010). Preparation of chitosan/magnetite composite beads and their application for removal of Pb(II) and Ni(II) from aqueous solution. *Materials Science and Engineering C*, *30*, 304–310.

Varma, A. J., Deshpande, S. V., & Kennedy, J. F. (2004). Metal complexation by chitosan and its derivatives: A review. *Carbohydrate Polymers*, *55*, 77–93.

Wang, L., & Wang, A. (2008). Adsorption properties of congo red from aqueous solution onto N,O-carboxymethyl-chitosan. *Bioresource Technology*, *99*, 1403–1408.

Wang, L. Y., Bao, J., Wang, L., Zhang, F., & Li, Y. D. (2006). One-pot synthesis and bioapplication of amine-functionalized magnetite nanoparticles and hollow nanospheres. *Chemistry – A European Journal*, *12*, 6341–6347.

Wan Ngah, W. S., & Fatinathan, S. (2010). Pb(II) biosorption using chitosan and chitosan derivatives beads: Equilibrium, ion exchange and mechanism studies. *Journal of Environmental Sciences*, *22*, 338–346.

Wan Ngah, W. S., Teong, L. C., & Hanafiah, M. A. K. M. (2011). Adsorption of dyes and heavy metal ions by chitosan composites: A review. *Carbohydrate Polymers*, *83*, 1446–1456.

Wu, F. C., Tseng, R. L., & Juang, R. S. (2001). Kinetic modeling of liquid-phase adsorption of reactive dyes and metal ions on chitosan. *Water Research*, *35*, 613–618.

Xie, G. R., Shang, X. Q., Liu, R. F., Hu, J., & Liao, S. F. (2011). Synthesis and characterization of a novel amino modified starch and its adsorption properties for Cd(II) ions from aqueous solution. *Carbohydrate Polymers*, *84*, 430–438.

Xu, F. Q., Zhang, N. N., Long, Y., Si, Y. M., Liu, Y., Mi, X., et al. (2011). Porous CS monoliths and their adsorption ability for heavy metal ions. *Journal of Hazardous Materials*, *188*, 148–155.

Yan, H., Yang, L. Y., Yang, Z., Yang, H., Li, A. M., & Cheng, R. S. (2012). Preparation of chitosan/poly(acrylic acid) magnetic composite microspheres and applications in the removal of copper(II) ions from aqueous solutions. *Journal of Hazardous Materials*, *229*, 371–380.

Zhou, L. M., Wang, Y. P., Liu, Z. R., & Huang, Q. W. (2009). Characteristics of equilibrium, kinetics studies for adsorption of Hg(II), Cu(II), and Ni(II) ions by thiourea-modified magnetic chitosan microspheres. *Journal of Hazardous Materials*, *161*, 995–1002.

Zhu, H. Y., Fu, Y. Q., Jiang, R., Yao, J., Xiao, L., & Zeng, G. M. (2012). Novel magnetic chitosan/poly(vinyl alcohol) hydrogel beads: Preparation, characterization and application for adsorption of dye from aqueous solution. *Bioresource Technology*, *105*, 24–30.

Zhu, Y. H., Hu, J., & Wang, J. L. (2012). Competitive adsorption of Pb(II), Cu(II) and Zn(II) onto xanthate-modified magnetic chitosan. *Journal of Hazardous Materials*, *221–222*, 155–161.